High-fidelity quantum sensing of magnon excitations with a single electron spin in quantum dots

Le-Tian Zhu(朱乐天)[1], Tao Tu(涂涛)[1,2,†], Ao-Lin Guo(郭奥林)[1], and Chuan-Feng Li(李传锋)[1,2,‡]

[1] *Key Laboratory of Quantum Information, University of Science and Technology of China, Chinese Academy of Sciences, Hefei* 230026, *China*
[2] *Hefei National Laboratory, University of Science and Technology of China, Chinese Academy of Sciences, Hefei* 230088, *China*

(Received 6 June 2022; revised manuscript received 5 August 2022; accepted manuscript online 12 August 2022)

Single-electron spins in quantum dots are the leading platform for qubits, while magnons in solids are one of the emerging candidates for quantum technologies. How to manipulate a composite system composed of both systems is an outstanding challenge. Here, we use spin–charge hybridization to effectively couple the single-electron spin state in quantum dots to the cavity and further to the magnons. Through this coupling, quantum dots can entangle and detect magnon states. The detection efficiency can reach 0.94 in a realistic experimental situation. We also demonstrate the electrical tunability of the scheme for various parameters. These results pave a practical pathway for applications of composite systems based on quantum dots and magnons.

Keywords: quantum sensing, magnons excitations, spin qubits in quantum dots

PACS: 03.67.Lx, 42.50.Dv, 42.50.Pq **DOI:** 10.1088/1674-1056/ac8919

1. Introduction

Magnons in ferromagnets are promising solid-state platforms for building interfaces between different quantum systems, which play an important role in various quantum information applications.[1] Using magnon mode conduction or virtual magnon exchange in spin chains, the robust transfer of quantum information between different nodes and the long-range entanglement between qubits can be achieved.[2–6] Using the coupling between magnon modes and different quantum components, quantum hybrid architectures can be realized, which is an attractive pathway to future scalable quantum processors.[7–10]

Electron spins in semiconductor quantum dots are one of the most promising candidates for qubits.[11,12] Because they are compatible with conventional semiconductor technology, quantum dots are leading the way in terms of large-scale fabrication and integration.[13,14] In purified silicon materials, electron spins exhibit long coherence times of up to 100 μs because the effect of surrounding nuclear spins is suppressed. Quantum dots have excellent gate controllability, so both single-qubit and two-qubit operations can be implemented with high fidelity in an electrical manner.[15–18] Recent significant advances include demonstration of demanding and complex quantum algorithms, such as variational quantum algorithm for calculating molecular energies, on a programmable quantum dot spin processor.[18,19]

The magnetic dipole moment of a single electron spin in quantum dots is small, so it couples weakly to the external magnetic excitations. On the one hand, this is an advantage for electron spin to maintain a long coherence time even in complex solid-state environments. On the other hand, this also makes it difficult to couple and control the magnetic excitations. Therefore, how to develop quantum dots for applications in the field of magnons has been an outstanding challenge.

Among the various quantum dot structures, double quantum dot systems have received more attention. In double quantum dots, in addition to the spin degree of freedom, the electron also has the orbital degree of freedom, such as the delocalization of the electron across the two quantum dots. The presence of orbital degrees of freedom enables the electron to have a large electric dipole moment. The control of the detuning and tunneling between the two quantum dots allows the tunability of the electric dipole moment. In this way, strong coupling to external control fields or other qubits can be obtained when needed. Thus, the additional charge degrees of freedom in the double quantum dot provide an effective interface between the electron and other systems. Based on double quantum dots, a number of impressive progresses have been made recently, such as achieving 99.5% measurement fidelity, the highest value reported so far in any solid-state spin system.[20,21]

In this article, we propose a scheme to combine quantum dots and magnons by using spin–charge hybridization. We focus on a single electron in a double quantum dot. In addition to having spin degree of freedom, it also has orbital degree of freedom, so it is a spin–charge hybrid system. Since the charge state has an electric dipole moment, it gives rise to a large coupling between the spin state and the external cavity field. Further, using the cavity field as an mediator, effective interaction between single electron spin and magnetic excitations can be achieved. Therefore, quantum dots can be used

†Corresponding author. E-mail: tutao@ustc.edu.cn
‡Corresponding author. E-mail: cfli@ustc.edu.cn

© 2022 Chinese Physical Society and IOP Publishing Ltd

for entanglement with magnetic modes and for the detection of magnon excitations. Our analysis shows that the detection efficiency is as high as 0.94 even in the presence of realistic noises and imperfections. We note that the readout efficiency is only about 0.1–0.5 in the experiments using optical methods to manipulate spin-wave excitations in solids as a quantum memory due to various noise effects.[22,23] These results provide opportunities for a wide range of applications using quantum dots to manipulate magnetic excitations.

2. The hybrid system

2.1. Spin-charge hybridization in the quantum dots

As shown in Fig. 1(a), we first consider a single electron confined in two quantum dots.[24–27] The electron has two basic orbital states of $|L\rangle$ and $|R\rangle$, and two basic spin states of $|\uparrow\rangle$ and $|\downarrow\rangle$. The potential difference between the two dots is ε and the tunnel coupling between the two dots is t_c. Both parameters can be adjusted by the voltage applied to the quantum dots. In addition to an overall external magnetic field B, a nearby micromagnet produces a magnetic field gradient ΔB between the two dots. This double-quantum dot system can be described by the Hamiltonian

$$H_{\rm qd} = \frac{\varepsilon}{2}\tilde{\tau}_z + t_c\tilde{\tau}_x + \frac{B}{2}\tilde{\sigma}_z + \frac{\Delta B}{2}\tilde{\tau}_z\tilde{\sigma}_x, \tag{1}$$

where $\tilde{\tau}_i$ and $\tilde{\sigma}_i$ are the Pauli matrices defined in the charge and spin subspaces, respectively.

In Fig. 1(b), we show the energy levels of the quantum dots as a function of the bias parameter ε. This is a four-level system with energy eigenvalues E_n and energy eigenstates $|n_{\rm qd}\rangle$. When $|\varepsilon|$ is large, the electron is localized in one quantum dot, whose energy eigenstates can be described as $|L,\downarrow\rangle$, $|L,\uparrow\rangle$, $|R,\downarrow\rangle$, $|R,\uparrow\rangle$. In contrast, when ε is near the avoided crossing point $\varepsilon \approx 0$, the electron is delocalized across the two quantum dots, forming the bonding and anti-bonding states $|-\rangle$, $|+\rangle$. Further, due to the presence of spin–orbit interactions (i.e., the last term in Eq. (1)), the bonding and anti-bonding states with opposite spins $|-,\uparrow\rangle$, $|+,\downarrow\rangle$ are hybridized, forming the energy eigenstates $|1_{\rm qd}\rangle$ and $|2_{\rm qd}\rangle$. While, the ground state is approximately unperturbed, leading to $|1_{\rm qd}\rangle \approx |-,\downarrow\rangle$. Thus, the spin states of the quantum dots depend on the charge states. The effective two-level Hamiltonian of the quantum dots can be written as

$$H_{\rm qd} = \frac{\omega_{\rm qd}}{2}\sigma_z, \tag{2}$$

where σ_i represents the Pauli matrices defined in the basis of spin–charge hybridized states of $|0_{\rm qd}\rangle$ and $|1_{\rm qd}\rangle$.

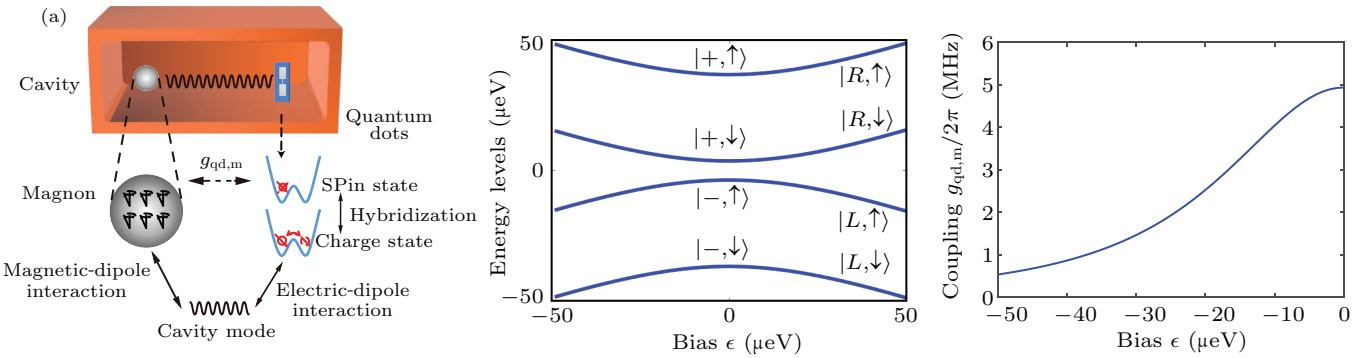


Fig. 1. (a) In the system we consider, there are three components: a single electron spin in the double quantum dot, a microwave mode in the cavity, and a magnon excitation in the magnet. The single spin and the cavity mode are coupled by an electric dipole interaction, labeled as $g_{{\rm qd},p}$. The magnon mode and the cavity mode are coupled by a magnetic dipole interaction, labeled as $g_{{\rm m},p}$. In this way the cavity mode acts as an intermediator, allowing an effective coupling $g_{\rm qd,m}$ between the single spin and the magnon mode. Here the double quantum dot is a double potential well structure. On the one hand, adjusting the voltage of the side gate can change the shape of the confinement potential, so that the electron is confined to either the left quantum dot or the right quantum dot, labeled as $|L\rangle$ and $|R\rangle$. On the other hand, adjusting the voltage of the middle gate can change the barrier height between the two quantum dots, so that the electron can tunnel between the two quantum dots. (b) Energy levels of quantum dots vs bias ε. (c) Effective coupling strength between quantum dots and magnons vs bias ε. Here we use the parameters as $t_c = 20$ μeV, $B = 33$ μeV, $\Delta B = 2$ μeV, $\omega_{\rm m}/2\pi = 7.92$ GHz, $\omega_p/2\pi = 8.45$ GHz, and $g_{{\rm m},p}/2\pi = 22.9$ MHz.

2.2. Spin–photon coupling between the quantum dots and the cavity

Then we consider a microwave cavity with the Hamiltonian

$$H_p = \sum_p \omega_p a_p^+ a_p, \tag{3}$$

where a_p^+ and a_p are the cavity photon operators. In the original basis of $|L\rangle$ and $|R\rangle$, the interaction between the quantum dots and the cavity can be described by

$$H_{{\rm qd},p} = g_{{\rm c},p}\tilde{\tau}_z(a_p + a_p^+), \tag{4}$$

where the electric dipole moment operator is $\tilde{\tau}_z = |L\rangle\langle L| - |R\rangle\langle R|$. Thus, in the new basis of of $|0_{\rm qd}\rangle$ and $|1_{\rm qd}\rangle$, the interaction Hamiltonian can be rewritten as

$$H_{{\rm qd},p} = \sum_p g_{{\rm qd},p}\sigma_x(a_p + a_p^+), \tag{5}$$

where the coupling strength is $g_{{\rm qd},p} = \langle 0_{\rm qd}|\tilde{\tau}_z|1_{\rm qd}\rangle g_{{\rm c},p}$. In this way, the combination of electric dipole moment and spin–

charge hybridization can lead to a large spin–cavity coupling $g_{\mathrm{qd},p}$.

2.3. Spin–magnon effective coupling between the quantum dots and the magnons

We now consider a hybrid system that consists of a yttrium iron garnet (YIG) ferromagnetic crystal and a double quantum dot, both coupled to the same microwave cavity, as illustrated in Fig. 1. Our system hosts three subsystems: the magnon modes in the magnetically ordered crystal can be depicted as

$$H_{\mathrm{m}} = \omega_{\mathrm{m}} c^{+} c, \tag{6}$$

where c^{+} and c are the creation and annihilation operators of magnons; the quantum dots and the microwave cavity are described by Eqs. (2) and (3), respectively. On the one hand, the magnetic modes can be coupled to the cavity with a coupling strength of $g_{\mathrm{m},p}$,[8]

$$H_{\mathrm{m},p} = \sum_{p} g_{\mathrm{m},p}(c^{+} a_p + c a_p^{+}). \tag{7}$$

On the other hand, the quantum dots are coupled to the cavity through the spin–charge hybridization with a coupling strength $g_{\mathrm{qd},p}$, as described in Eq. (5). Thus, using the cavity as a mediator, these interactions lead to an effective coupling between the magnetic modes and the quantum dots. When the frequency of the cavity is far detuned from those of the quantum dots and the magnetic modes, the effective interaction between the quantum dots and the magnetic modes can be described as

$$H_{\mathrm{qd,m}} = g_{\mathrm{qd,m}}(\sigma_{+} c + \sigma_{-} c^{+}). \tag{8}$$

Here the effective coupling strength is given by

$$g_{\mathrm{qd,m}} = \sum_{p} \frac{g_{\mathrm{qd},p} g_{\mathrm{m},p}}{\omega_{\mathrm{m}} - \omega_p}. \tag{9}$$

As shown in Fig. 1(c), the value of the coupling strength $g_{\mathrm{qd,m}}$ can increase by a factor of 5 when the bias of the quantum dots ε is changed from the large detuning regime to the near avoided crossing regime. This result is due to the fact that changing the bias voltage can change the electron from being localized in one quantum dot to being delocalized across the two quantum dots. This increases the charge distribution length of the electron and thus enhances its electric dipole moment, leading to a large electric dipole interaction $g_{\mathrm{qd},p}$. In this way, adjusting the bias ε changes the coupling strength $g_{\mathrm{qd},p}$ of the quantum dots to the cavity, which further changes the coupling strength $g_{\mathrm{qd,m}}$ of the quantum dots to the magnons.

Furthermore, when the frequency of the quantum dots is detuning from the frequency of the magnetic modes, the interaction Hamiltonian can be reduced as

$$H_{\mathrm{qd,m}} = \chi_{\mathrm{qd,m}} c^{+} c \sigma_z. \tag{10}$$

Here $\chi_{\mathrm{qd,m}} = g_{\mathrm{qd,m}}^2/(\omega_{\mathrm{qd}} - \omega_{\mathrm{m}})$ characterizes the shift of the energy levels of quantum dots due to the presence of magnetic modes.

3. Quantum sensing scheme of the magnons

As shown in Fig. 2(a), the scheme for controlling and detecting magnetic modes using quantum dots is designed as follows:

(i) First, the state of the magnetic excitations is prepared, which is a superposition state of magnon Fock states

$$|\Psi_{\mathrm{m}}\rangle = \sum_{n} c_n |n_{\mathrm{m}}\rangle. \tag{11}$$

Meanwhile, the quantum dots are prepared in the ground state.

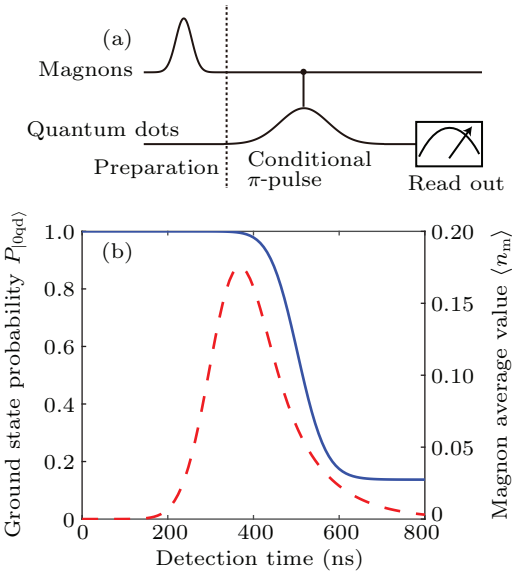


Fig. 2. (a) Schematic diagram of the scheme for detecting the magnon states. (b) Dynamics of the protocol for detecting the magnon states. Here the red dashed line shows the expectation value of the magnons $\langle n_{\mathrm{m}}\rangle$, and the blue solid line shows the probability of the quantum dots in the ground state $P_{|0_{\mathrm{qd}}\rangle}$. Here we use the pulse parameter of magnons $\Omega_{\mathrm{m}}/2\pi = 0.8$ MHz, the pulse parameter of quantum dots $\Omega_{\mathrm{qd}}/2\pi = 1.25$ MHz, and the other parameters as in Fig. 1.

(ii) As described in Eq. (10), the frequency of the quantum dots is shifted by the magnetic modes and therefore depends on the state of the magnetic modes. This magnon-state-dependent frequency shift is the key to the present scheme. A π-pulse is applied to the quantum dots, whose operating frequency corresponds to the frequency of the quantum dots, when the magnetic modes are in the vacuum state $|0_{\mathrm{m}}\rangle$. By applying such a conditional π-pulse, the state of the composite system becomes

$$P_{\pi}|0_{\mathrm{qd}}\Psi_{\mathrm{m}}\rangle = c_0|1_{\mathrm{qd}}0_{\mathrm{m}}\rangle + \sum_{n>0} c_n |0_{\mathrm{qd}} n_{\mathrm{m}}\rangle. \tag{12}$$

(iii) The above equation suggests that the state of the quantum dots and the state of the magnetic modes are entangled after the application of the π-pulse. The probability that

the quantum dots are in the excited state indicates that the magnetic modes are in the vacuum state $|0_{\rm m}\rangle$, while the probability that the quantum dots are in the ground state indicates that the magnetic modes are in the magnon number state $|n_{\rm m}\rangle$. Therefore, using standard techniques to measure the quantum dots provides information about the magnetic modes.

4. The models and simulations of the hybrid system

To demonstrate this manipulation and detection scheme, we perform numerical simulation of dynamics of the whole system. In the rotating frame of the quantum dot and the magnon frequencies, the Hamiltonian of the composite system can be written as

$$\begin{aligned} H_t &= H_{\rm qd}+H_{\rm m}+H_{\rm qd,m}+H_{\rm qd}^{c}++H_{\rm m}^{c} \\ &= \frac{\Delta_{\rm qd}}{2}\sigma_z+\Delta_{\rm m}c^{+}c+\chi_{\rm qd,m}c^{+}c\sigma_z \\ &\quad +\Omega_{\rm qd}(t)\sigma_x+\Omega_{\rm m}(t)(c+c^{+}). \end{aligned} \tag{13}$$

Here $\Delta_{\rm qd}=\omega_{\rm qd}-\omega_{\rm d}$ and $\Delta_{\rm m}=\omega_{\rm m}-\omega_{\rm d}$ are the detuning of the quantum dot frequency and magnon frequency from the control pulse frequency, respectively. The last two terms in the Hamiltonian represent the control pulse fields applied to the quantum dots and the magnons, respectively. The dynamics of the system is determined by the master equation

$$\frac{{\rm d}\rho}{{\rm d}t}=-{\rm i}[H_t,\rho]+\sum_k \gamma_k L_k[\rho], \tag{14}$$

where each dissipation process is described by the Lindblad operator $L_k[\rho]=L_k\rho L_k^{+}-\frac{1}{2}L_k^{+}L_k\rho-\frac{1}{2}\rho L_k^{+}L_k$ with a rate γ_k. For this composite system, we consider three main dissipative processes: the spin relaxation process of quantum dots, whose corresponding operator is $L_k=\sigma_-$ with a rate $\gamma_1=\frac{1}{T_1}$; the spin dephasing process of quantum dots, whose corresponding operator is $L_k=\sigma_z$ with a rate $\gamma_\phi=\frac{1}{T_\phi}$; and the relaxation process of magnons, whose corresponding operator is $L_k=c$ with a rate $\gamma_{\rm m}=\frac{1}{T_{\rm m}}$. Here we use the parameter values extracted from the experiments: the relaxation time $T_1=1.2$ ms and the dephasing time $T_\phi=0.8$ μs for quantum dots,[19,24] and the relaxation time $T_{\rm m}=110$ ns for magnons.[10]

The calculation of the master equation requires long time resources because of the large state space of the hybrid system. Therefore, we derive the equations of motion for the expectation values of the operators of the hybrid system. From the master equation, we can obtain a series of coupled equations involved high order moments. Then, we factor the higher order terms into the first order terms, e.g., $\langle c\sigma_z\rangle\simeq\langle c\rangle\langle\sigma_z\rangle$. This is a good approximation because the dynamics of the magnons in the hybrid system is dominated by the expectation value and the fluctuation is small. In this way, we obtain the following equation of motion for the hybrid system:

$$\frac{{\rm d}\langle c\rangle}{{\rm d}t}=-{\rm i}\Delta_{\rm m}\langle c\rangle-{\rm i}\chi_{\rm qd,m}\langle c\rangle\langle\sigma_z\rangle-{\rm i}\Omega_{\rm m}-\frac{\gamma_{\rm m}}{2}\langle c\rangle, \tag{15}$$

$$\frac{{\rm d}\langle\sigma_z\rangle}{{\rm d}t}=\Omega_{\rm qd}\langle\sigma_y\rangle-\gamma_1(\langle\sigma_z\rangle+1), \tag{16}$$

$$\begin{aligned} \frac{{\rm d}\langle\sigma_x\rangle}{{\rm d}t} &= -(\Delta_{\rm qd}+2\chi_{\rm qd,m}\langle c^{+}\rangle\langle c\rangle+\chi_{\rm qd,m})\langle\sigma_y\rangle \\ &\quad -{\rm i}\chi_{\rm qd,m}\langle c\rangle\langle\sigma_z\rangle-\left(\frac{\gamma_1}{2}+\gamma_\phi\right)\langle\sigma_x\rangle, \end{aligned} \tag{17}$$

$$\begin{aligned} \frac{{\rm d}\langle\sigma_y\rangle}{{\rm d}t} &= (\Delta_{\rm qd}+2\chi_{\rm qd,m}\langle c^{+}\rangle\langle c\rangle+\chi_{\rm qd,m})\langle\sigma_x\rangle \\ &\quad -{\rm i}\chi_{\rm qd,m}\langle c\rangle\langle\sigma_y\rangle-\left(\frac{\gamma_1}{2}+\gamma_\phi\right)\langle\sigma_y\rangle-\Omega_{\rm qd}\langle\sigma_z\rangle. \end{aligned} \tag{18}$$

In the simulations, we numerically solve this set of coupled differential equations. Moreover, we find that the results of the equation of motion are consistent with those of the master equation, which indicates that our factorization approximation captures the underlying dynamical structure of the hybrid system.

5. Quantum sensing results

5.1. Detection process

We use the scheme to detect the coherent state of magnons. First, we apply a driving pulse to the ferromagnet to prepare the coherent state of magnons $|\Psi_{\rm m}\rangle=|\alpha\rangle$. Second, after a delay time of $t_{\rm d}=200$ ns, we apply a Gaussian-shaped π pulse to the quantum dots to generate an entangled state of the quantum dots and the magnons. Finally, we measure the probability of the quantum dots in the ground state $P_{|0_{\rm qd}\rangle}$.

In Fig. 2(b), we plot the time evolution of the expectation value of magnons $\langle n_{\rm m}\rangle=\langle\Psi_{\rm m}|c^{+}c|\Psi_{\rm m}\rangle$ as well as the ground state population of the quantum dots $P_{|0_{\rm qd}\rangle}$. In the first stage, the expectation value of magnons increases with time and reaches a peak, indicating the preparation of the coherent state of magnons. Here, the magnon excitation is prepared by microwave pulses with a peak value of $\langle n_{\rm m}\rangle=0.18$. In this stage the quantum dots remain in the initial ground state and do not change. In the second stage, the state of the quantum dots starts to respond to the magnons due to the application of the conditional π pulse, which allows the quantum dots to be entangled with the magnons. The ground state population of the quantum dots continues to decrease and reaches a steady value. In this case, the population of quantum dots $P_{|0_{\rm qd}\rangle}$ significantly changes from the initial value of 1 to the final value of 0.14 due to the entanglement of quantum dot spins and magnons. This final ground state population corresponds to the probability of the magnon state $|n_{\rm m}\rangle$.

5.2. Detection efficiency for the magnon coherent states

We further demonstrate the detection of various coherent states of magnons. First, we prepare the coherent states of

magnons with different amplitudes $|\alpha|^2$. The coherent state can be expressed as $|\alpha\rangle = \sum_n c_n |n_{\rm m}\rangle$, where the superposition coefficient is $c_n = {\rm e}^{-\frac{1}{2}|\alpha|^2}\frac{\alpha^n}{\sqrt{n!}}$. In addition, the expectation value of magnons for a coherent state $|\alpha\rangle$ is $\langle n_{\rm m}\rangle = |\alpha|^2$. Second, after applying the conditional π-pulse, the entangled state of the composite system can be expressed as $c_0|1_{\rm qd}0_{\rm m}\rangle + \sum_{n>0} c_n|0_{\rm qd}n_{\rm m}\rangle$. In particular, the first superposition factor is $c_0 = {\rm e}^{-\frac{1}{2}|\alpha|^2}$, which means that the excited state population of the quantum dots is $P_{|1_{\rm qd}\rangle} = |c_0|^2 = {\rm e}^{-|\alpha|^2}$. In this way, the ground state population of the quantum dots is $P_{|0_{\rm qd}\rangle} = 1 - |c_0|^2 = 1 - {\rm e}^{-|\alpha|^2}$, which has a simple scaling law with respect to the expectation value of magnons $P_{|0_{\rm qd}\rangle} = 1 - {\rm e}^{-\langle n_{\rm m}\rangle}$.

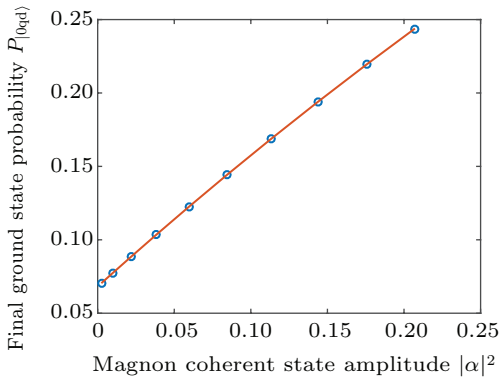


Fig. 3. Probability of the quantum dots in the ground state as a function of the amplitude $|\alpha|^2$ of the magnon coherent state. The circles are simulation results and the solid line is the fit to extract the efficiency. Here we use the same parameters as in Fig. 2.

In Fig. 3, we simulate the ground state probability of the quantum dots for different magnon coherent states. The solid line in the figure is the fitted equation: $P_{|0_{\rm qd}\rangle} = \eta(1 - {\rm e}^{-\langle n_{\rm m}\rangle}) + d$. Here η and d denote the efficiency and dark-count rate of the detection process, respectively. In the ideal case, the efficiency $\eta = 1$ and the dark count rate $d = 0$, where the detection results reduce to a simple scaling law $1 - {\rm e}^{-\langle n_{\rm m}\rangle}$. However, the state of the quantum dots is subject to the decoherence effects from the environment, which limits the efficiency $\eta < 1$ of the detection process. In addition, decoherence from the environment causes changes in the quantum dot state even in the absence of magnons, which gives rise to an incorrect detection result, i.e., the dark count rate $d > 0$ of the detection process. Using the fit in Fig. 3, we can obtain two performance metrics for the detection process in a realistic environment as $\eta = 0.94$ and $d = 0.06$, when the magnons are in the state $|n_{\rm m}\rangle$.

5.3. Detection efficiency with respect to various system parameters

To explore the limitation factors of the present scheme, we investigate the effect of decoherence parameters on the detection efficiency. In Fig. 4(a), we find that the detection efficiency η increases with the increase of the relaxation time T_1 and the dephasing time T_ϕ of the quantum dots. For example, for a fixed relaxation time $T_1 = 25$ μs, when the dephasing time T_ϕ is varied from 100 ns to 4 μs, the detection efficiency increases rapidly from the lower value of 0.1 to close to the ideal value of 1. This result is expected because in this scheme, the quantum dots serve as sensors whose quantum coherence time determines the detection efficiency. Further, we find that the detection efficiency η increases more significantly with the dephasing time T_ϕ than with the relaxation time T_1. Because the key of this quantum sensing scheme is to generate the entangled states between the quantum dots and the magnons, it is more significantly affected by the dephasing process.

We also investigate the detection efficiency by varying the operation time of the conditional π pulse. In Fig. 4(b), we find that the detection efficiency η gradually decreases with the increase of the duration t_p of the π pulse. For example, when the operation time increases to 400 ns, which is comparable to the dephasing time T_ϕ of quantum dots, the detection efficiency drops to a lower value of 0.76. This result is also anticipated because the total measurement time increases as the π pulse duration increases, the decoherence effect starts to play a significant role, leading to a decrease in detection efficiency. Ideally, if the pulse duration is very short, the detection efficiency can be close to 1. However, under practical experimental conditions, it is difficult to implement fast pulse or short pulse duration. Therefore, this result motivates the design of optimized pulse sequences to achieve higher detection efficiency in future work.

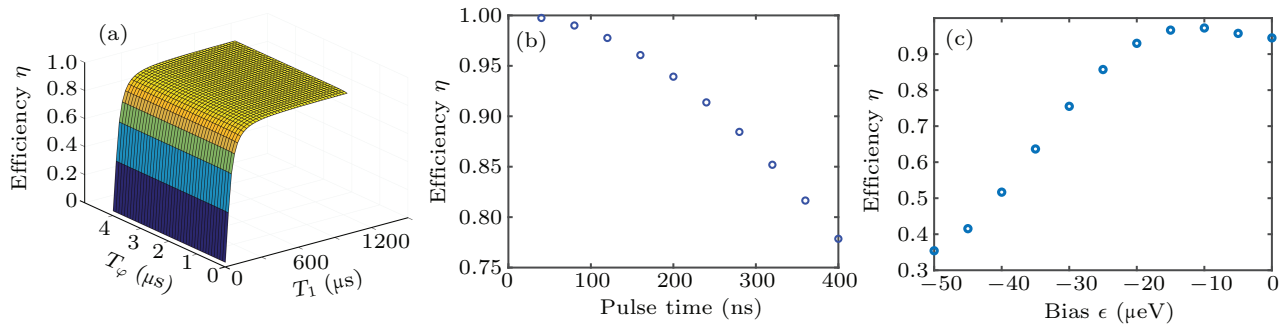


Fig. 4. (a) Detection efficiency as a function of relaxation time T_1 and dephasing time T_ϕ. (b) Detection efficiency as a function of π-pulse operating time t_p. (c) Detection efficiency as a function of quantum dot bias ε. Here we use the same parameters as in Fig. 2.

In Fig. 4(c), we find that the detection efficiency changes substantially as the bias ε of the quantum dots changes. The detection efficiency increases significantly from a lower value of 0.3 to a higher value close to 1 when the bias voltage of the quantum dots is changed from the large detuning regime to the near avoided crossing regime. This result is consistent with the electrical tunability result of Fig. 1(c). As shown in Fig. 1(c), the effective coupling strength $g_{\mathrm{qd,m}}$ between quantum dots and magnons can be electrically tuned over a wide range by the bias parameter ε, leading to a greater strength of interaction between quantum dots and magnons, thus resulting in the higher detection efficiency shown in Fig. 4(c). This result indicates that our scheme has rich electrical tunability compared to other quantum sensing schemes.

6. Conclusions

In summary, we propose a scheme for the control and detection of magnetic excitation modes in ferromagnets using quantum dots. In a realistic solid state environment, the detection efficiency can reach a high value of 0.94. This efficiency value is several times larger than the state-of-art spin-wave readout efficiency value using optical methods.[22,23] Our analysis shows that decoherence effects limit the performance of the scheme, so detection efficiency can be further improved by designing optimal working points or using composite pulses.[28–30] Here we demonstrate the detection of magnetic coherent states, it would be interesting to design quantum non-demolition measurement protocols, which could enable richer detection methods.[31] In addition, the scheme can be used for the selective generation of magnon states, which is a crucial step toward the magnon-based quantum technologies. In the future, these schemes can be used to probe exotic magnetic excitations in various solid materials, and to develop quantum technology applications for composite quantum systems.

Acknowledgements

Project supported by the National Natural Science Foundation of China (Grant No. 11974336) and the National Key Research and Development Program of China (Grant No. 2017YFA0304100).

References

[1] Kurizki G, Bertet P, Kubo Y, Molmer K, Petrosyan D, Rabl P and Schmiedmayer J 2015 *Proc. Natl. Acad. Sci. USA* **112** 3866
[2] Trifunovic L, Pedrocchi F L and Loss D 2013 *Phys. Rev. X* **3** 041023
[3] Neuman T, Wang D S and Narang P 2020 *Phys. Rev. Lett.* **125** 247702
[4] van der Sar T, Casola F, Walsworth R and Yacoby A 2015 *Nat. Commun.* **6** 7886
[5] Du C, van der Sar T, Zhou T X, Upadhyaya P, Casola F, Zhang H, Onbasli M C, Ross C A, Walsworth R L and Tserkovnyak Y and Yacoby A 2017 *Science* **357** 195
[6] Andrich P, Charles F, Liu X, Bretscher H L, Berman J R, Heremans F J, Nealey P F and Awschalom D D 2017 *npj Quantum Inf.* **3** 28
[7] Tabuchi Y, Ishino S, Noguchi A, Ishikawa T, Yamazaki R, Usami K and Nakamura Y 2015 *Science* **349** 405
[8] Tabuchi Y, Ishino S, Noguchi A, Ishikawa T, Yamazaki R, Usami K and Nakamura Y 2016 *C. R. Phys.* **17** 729
[9] Lachance-Quirion D, Tabuchi Y, Gloppe A, Usami K and Nakamura Y 2019 *Appl. Phys. Express* **12** 070101
[10] Lachance-Quirion D, Wolski S P, Tabuchi Y, Kono S, Usami K and Nakamura Y 2020 *Science* **367** 425
[11] Awschalom D D, Bassett L C, Dzurak A S, Hu E L and Petta J R 2013 *Science* **339** 1174
[12] Kloeffel C and Loss D 2013 *Annu. Rev. Condens. Matter Phys.* **4** 51
[13] Vandersypen L M K, Bluhm H, Clarke J S, Dzurak A S, Ishihara R, Morello A, Reilly D J, Schreiber L R and Veldhorst M 2017 *npj Quantum Inf.* **3** 34
[14] Xue X, *et al.* 2021 *Nature* **593** 205
[15] Yoneda J, Takeda K, Otsuka T, Nakajima T, Delbecq M R, Allison G, Honda T, Kodera T, Oda S, Hoshi Y, Usami N, Itoh K M and Tarucha S 2018 *Nat. Nanotechnol.* **13** 102
[16] Yang C H, Chan K W, Harper R, Huang W, Evans T, Hwang J C C, Hensen B, Laucht A, Tanttu T, Hudson F E, Flammia S T, Itoh K M, Morello A, Bartlett S D and Dzurak A S 2019 *Nat. Electron.* **2** 151
[17] Noiri A, Takeda K, Nakajima T, Kobayashi T, Sammak A, Scappucci G and Tarucha S 2022 *Nature* **601** 338
[18] Xue X, Russ M, Samkharadze N, Undseth B, Sammak A, Scappucci G and Vandersypen L M K 2022 *Nature* **601** 343
[19] Watson T F, Philips S G J, Kawakami D R, Ward E, Scarlino P, Veldhorst M, Savage D E, Lagally M G, Friesen M, Coppersmith S N, Eriksson M A and Vandersypen L M K 2018 *Nature* **555** 633
[20] Nakajima T, Delbecq M R, Otsuka T, Stano P, Amaha S, Yoneda J, Noiri A, Kawasaki K, Takeda K, Allison G, Ludwig A, Wieck A D, Loss D and Tarucha S 2017 *Phys. Rev. Lett.* **119** 017701
[21] Takeda K, Noiri A, Yoneda J, Nakajima T and Tarucha S 2020 *Phys. Rev. Lett.* **124** 117701
[22] Gundogan M, Ledingham P M, Kutluer K, Mazzera M and de Riedmatten H 2015 *Phys. Rev. Lett.* **114** 230501
[23] Jobez P, Usmani I, Timoney N, Laplane C, Gisin N and Afzelius M 2014 *New J. Phys.* **16** 083005
[24] Mi X, Benito M, Putz S, Zajac D M, Taylor J M, Burkard G and Petta J R 2018 *Nature* **555** 599
[25] Lin Z R, Guo G P, Tu T, Zhu F Y and Guo G C 2008 *Phys. Rev. Lett.* **101** 230501
[26] Wang L, Tu T, Gong B and Guo G C 2015 *Phys. Rev. A* **92** 062346
[27] Zhu X. Y, Tu T, Guo A L, Zhou Z Q and Guo G C 2020 *Chin. Phys. Lett.* **37** 020302
[28] Zhou B B, Baksic A, Ribeiro H, Yale C G, Heremans F J, Jerger P C, Auer A, Burkard G, Clerk A A and Awschalom D D 2017 *Nat. Phys.* **13** 330
[29] Guo A L, Tu T, Guo G C and Li C F 2021 *Phys. Rev. A* **104** 022404
[30] Gong B, Tu T, Guo A L, Zhu L T and Li C F 2021 *Chin. Phys. Lett.* **38** 044201
[31] Kono S, Koshino K, Tabuchi Y, Noguchi A and Nakamura Y 2018 *Nat. Phys.* **14** 546